Advances in Science and Technology Research Journal

Advances in Science and Technology Research Journal 2023, 17(2), 330–341
https://doi.org/10.12913/22998624/161831
ISSN 2299–8624, License CC-BY 4.0

Received: 2023.01.06
Accepted: 2023.03.15
Published: 2023.04.01

Effect of Annealing Treatment on ($Mg_{17}Al_{12}$) Phase Characterization and Corrosion Behavior in Different Solutions for AZ91 Alloy

Marwa H. Abass[1], Makarim H. Abdulkareem[1*], Hussien A. Hussein[1]

[1] Department of Production Engineering and Metallurgy, University of Technology-Iraq, Baghdad, Iraq

* Corresponding author's e-mail: makarim.h.abulkareem@uotechnology.edu.iq

ABSTRACT

Heat treatment is the most suitable technique for altering the microstructure and, consequently, it is possible to create the optimal balance of corrosion resistance and mechanical strength in a material by carefully regulating the conditions during the heating process. The present work aims to investigate the effect of heat treatments (annealing) at 300 °C, at different times (10, 20, and 30 h) on the magnesium alloy. How the $Mg_{17}Al_{12}$ phase influences the corrosion behavior of AZ91D magnesium alloy was quantified in different solution (SBF, Lactic and Ringer). It was able to construct an extensive range of $Mg_{17}Al_{12}$ phase volume fractions by varying the annealing period. The corrosion potential of many specimens with varied proportions of the $Mg_{17}Al_{12}$ phase was evaluated. The results of the conducted tests manifested that the material's resistance to corrosion greatly improved with an increase in the volume fraction of $Mg_{17}Al_{12}$ phase. The effect of heat treatment on the microstructure was analyzed using transmission electron microscopy and X-ray diffraction. The SEM photographs evinced that the amount of β-$Mg_{17}Al_{12}$ phase decreased significantly, with the distribution occurring at the grain boundaries and with increasing the time of annealing, resulting in a highly saturated α-grain. The XRD validated the all material peaks of phases that are present. The corrosion test behavior of AZ91 alloy in the simulated body fluid (SBF), lactic, and Ringer solutions was investigated through electrochemical measurements, the result was elucidated as measured along the Tafel slope, and the corrosion current density of all heat treated samples was lower than that of the as-cast sample. The measurement of hardness (HV) demonstrated that the hardness decreased to 64.5 HV0.5 during the heat treatment. The result antibacterial efficiency was revealed that AZ91 at 30 hr was best then as cast against the bacteria E.coli.

Keywords: AZ91, heat treatment, corrosion, microstructure, antibacterial, hardness.

INTRODUCTION

Magnesium (Mg), which is the cation that is found in the human body the fourth most, is mainly deposited in the skeletal tissue (60–65%) and tissues that are sudpple and pliable (35–40%), and majority of it being kept in the muscle, which accounts for 27%. Currently, the Mg consumptions of 420 mg for men and 320 mg for women per day are advocated and recommended by the United States Food and Nutrition Council [1]. The Mg ions in excess can be sequestered in matrix structures inside cells or bone marrow forms, or they can be distributed throughout blood flow mechanics. To avoid the hypomagnesaemia, this is usually pursued by excretion in the urine [2].

Mg is a member of the effective metals group with low electrochemical potential, proposing a vigorous propensity for oxidation [3]. For this reason, pure Mg and its alloys are vulnerable to corrosion in the highly conductive atmospheres like the aqueous solutions due to their electrochemical activity. The low weight and ecological friendliness of Mg alloys, on the other hand, make them an interesting structural material selection [4]. Even yet, their utilization is still limited via their deprived ductility and strength, which makes them less appropriate for numerous uses [5].

Mg becomes progressively important in the dental, cardiovascular, and skeletal system hard tissue replacement uses. Metal-based implants can be made because Mg is biocompatible, has

mechanical characteristics that are extremely near to those of human bone, and the Mg ions have an acceleration impact on the bone healing, as opposed to the usual bio alloys [6]. Consequently, these alloys were created to eliminate the need for a second surgery for removing the implants after healing the fracture, since they deteriorate beneath the natural circumstances [7].

AZ91 alloy is the most broadly used cast Mg alloy due to its high strength, superior corrosion resistance, and high castability [8]. In this alloy, when increasing the aluminum (Al) concentration in chloride, the medium has a positive influence on the corrosion behavior although the process and the effect of aluminum remain ambiguous. AZ91 alloy has β-phase ($Mg_{17}Al_{12}$) at the grain boundaries as a continuous phase and a part of a lamellar structure as a portion of the incomplete solid solution phase. Corrosion resistance in the Mg-Al alloys is determined by β-phase ($Mg_{17}Al_{12}$) distribution [9].

Since the corrosion behavior in Mg-Al alloys is regulated by micro-galvanic cells generated between the cathode $Mg_{17}Al_{12}$ phase and the anodic α-Mg matrix, and regarding this topic, the importance of the volume fraction of the $Mg_{17}Al_{12}$ phase cannot be overstated [10]. The β-phase function in the corrosive process of Mg-Al alloys has been the topic of a significant amount of research and debate in the published works. Consequently, it is theoretically recognized that the β-phase, depending on its size and distribution, either functions as an effective cathode or as a barrier against corrosion [11].

Nevertheless, the Mg alloys frequently possess a high rate of deterioration and a quick loss of mechanical strength when tested in living organisms. As a result, attempts have been undertaken to slow down their fast degrading behavior by including non-toxic alloying elements, modifying the surface, undergoing heat treatment, using an amorphous alloy, and several other strategies [12]. There several method to improve surface of AZ91 such as improving by plasma electrolytic oxidation [13], electro spun polymer nanocomposite [14], electron beam processed[15], and electroless coating [16].

Without affecting the alloy's composition or physical form, heat treatment is the most efficient method for adjusting the microscopic organization by improving the mechanical properties and the corrosion behavior[17]. By carefully modifying the thermal treatment conditions, it is possible to achieve the optimal balance between corrosion resistance and mechanical strength. The aim of the present study is to determine the effect of heat treatment (annealing) at various times on the $Mg_{17}Al_{12}$ microstructure and corrosion behavior for the Mg AZ91 alloy after being exposed to different solutions, including the SPF, lactic, and Ringer solutions. The second goal of heat treatment is to increase the mechanical properties.

EXPERIMENTAL PROCEDURE

Used material

The chemical analysis of the used magnesium alloy AZ91 was conducted used Atomic absorption spectrophotometer-AA680-Shimadzo, Japan in (State Company for Inspection and Engineering Rehabilitation (S.I.E.R)/Ministry of Industry and Minerals, Iraq) to obtain its chemical composition as given in Table 1.

Sample preparation

Samples of Mg AZ91 alloy, with a dimension of 10×10×5 mm, were cut into 3 pieces prepared to be used in heat treatment. Each sample was then polished with 220–2000 abrasive papers without lubricants to minimize the effect of amorphous oxide formation.

Annealing treatment

In the annealing process, the samples of Mg AZ91 alloy were first placed in a crucible and then put in an electric furnace (Carbolite) at a temperature of 300 °C, with pumping inert argon gas at a rate of (1 liter per minute). These samples were then fixed at this temperature for different times (10, 20, and 30 hr) and finally cooled inside the furnace. The effect of annealing times on

Table 1. Chemical composition of magnesium alloy AZ91

Mg%	Al%	Zn%	Mn%	Fe%	Co%	Ga%	Nb%	Se%	Pd%
Bal.	8.97	0.58	0.32	0.01	0.003	0.006	0.002	0.001	0.003

improving the mechanical properties of the microstructure and corrosion was determined.

Microstructural examination

For the microstructure examination of Mg AZ91 alloy by Scanning Electron Microscope and optical microscope, samples were prepared after grinding them by emery papers having the following grits: 220, 400, 600, 1000, 1200, and 2000, respectively. After that, all samples were polished with cloth impregnated with fine alumina to obtain a smooth surface.

Microhardness test

Mg Alloy AZ91 was subjected to a Vickers hardness test (ZWICK Z313 – Germany). In this test, the weight was 0.5 kg applied for 15 s. Each sample was subjected to three measurements to determine the average diameter.

Corrosion tests

A polarized electrochemical examination was approved. All corrosion tests were conducted in Lactic acid, Ringer and SBF Solutions by a monitored device (PCI4/750, Warminster, Pennsylvania, GAMRY, Inc.). At 37 °C, and scan rate of electrochemical tests is 1 mv/s, the reference pole is Ag/AgCl, whereas both the auxiliary and main poles are made of precious metals (Pt). A lactic solution was applied to the specimen. The area of exposure measured was 1 mm^2. Prior to each examination, the samples were polished metallographically. Until a steady-open circuit potential was achieved, the samples were then submerged into the solution. The exposed area of the test specimens was about 10 mm^2. Each part of data was averaged out based on the total surface area. It was calculated with the help of the Echem analyzer to unambiguously identify the test results.

X-Ray Diffraction analysis

The X-ray diffraction Shimadzu (XRD-6000) diffractometer available in the Nanotechnology Center at the University of Technology was used to examine the phases of the modified Mg AZ91 alloy samples. The radius scanning is 185 mm, C, and NF (154060 nm) radio X-rays, and the radius leakage is less than 2.5 Sv/h at the maximum output.

Antibacterial activity test by zone inhibition method

Bacteria that can be categorized as either gram-negative or gram-positive (Ecoli and Staphylococcus) were tested, with samples taken from the Biotechnology Branch-Nanotechnology Center Laboratory. These bacteria were grown on "nutrient agar (N. agar)" and incubated for twenty four hr at 37°C in a temperature-controlled atmosphere. They were dissolved into 50 ml of normal saline solution to produce a "107 FU/ml" bacterial suspension, which was utilized as a control, and 100 ml of this solution were put on a nutrient agar plate for further analysis. Samples of polymers, mixes, and composites were placed into the plates to determine the inhibition zone. Eventually, these plates were incubated for some time at a temperature of 37°C. The zones of inhibition were determined following a 24-hour incubation period.

RESULTS AND DISCUSSION

Microstructure examination

The heat treatment modifies the microstructure of the specimens, as evinced in Figure 1 (The red color represents the volumetric fraction). The Mg alloys with less than 10%Al from the AZ (aluminum and zinc) class constitute a solid solution of Mg-Al. The $Mg_{17}Al_{12}$ phase crystallizes at the grain boundaries in the presence of Al concentrations greater than 1% at the ambient temperature. The maximum solubilization temperature for the Al is 437°C, where it achieves a solubility of 12.6% [18]. Mg and Al are mixed to generate a solid solution that results in the formation of granular grains. From Figure 1(a), it can be noted that the β-phase at the α-grains' margins in Mg AZ91 alloy creates a network-like structure, eutectic regions, where the both phases are present and can be observed adjacent to the β-phase areas. In particular, it was determined that the volume fraction of Mg AZ91 alloy annealed for 0 hr was 17.777. From Figure 1(b), it can be observed that the microstructure underwent a dramatic change after being heated for 10 hr. The eutectic zones which were a combination of α and β regions were eliminated. After the heat treatment for 10 hr, the eutectic zones disappeared after the solubility limit was raised

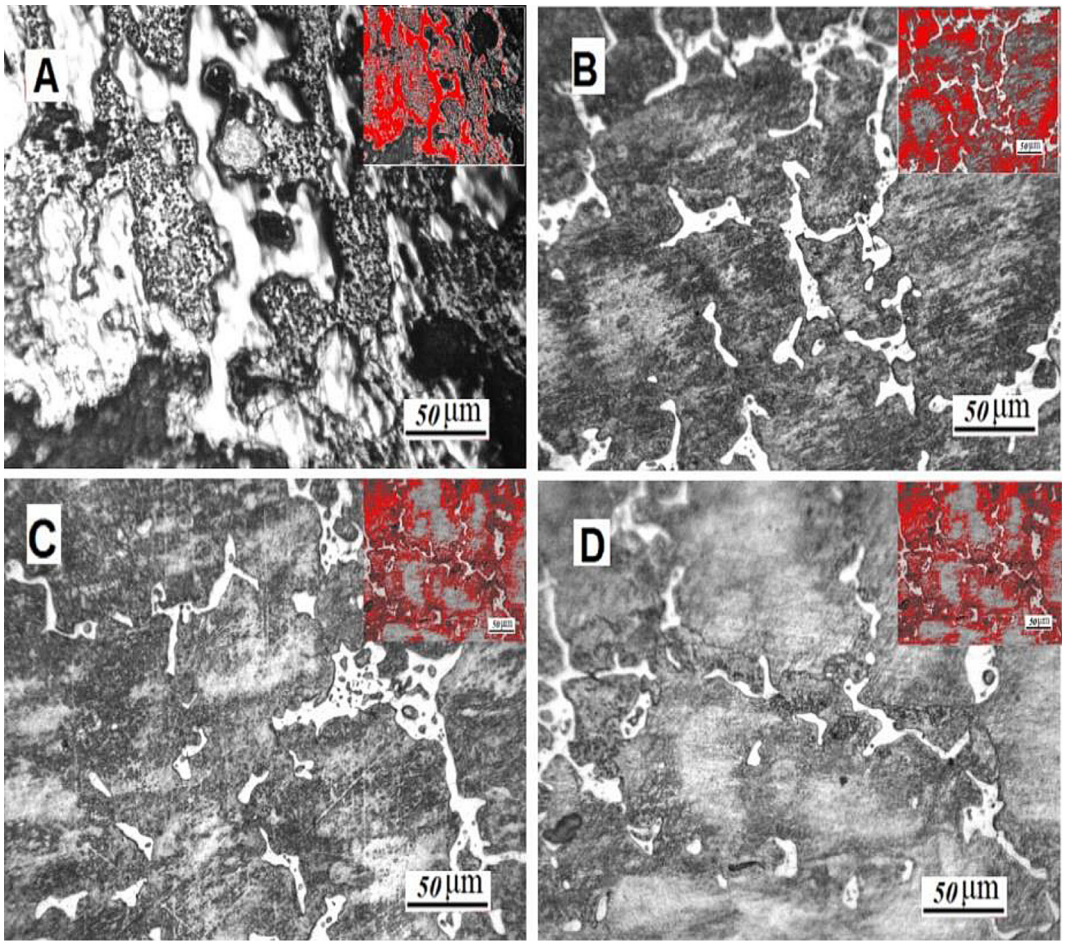

Figure 1. Microstructure of the AZ91 magnesium alloy: (a) 0 h; (b) 10 h; (c) 20 h; and (d) 30 h

to 300°C. Also, it is noticed in Figure 1(b), the Al supersaturation in some α-grains next to the β-phase rose to 20.175% by volume fraction. In addition, the microstructure after the annealing treatment for 20 hr revealed that the Al dissolved more easily and the volume fraction increased to 31.148%. The quantity and distribution of β-phase were drastically altered by the heating process. It is interesting to see that a clear boundary appeared after 10 and 20 hr of the annealing treatment. This boundary, as depicted in Figure 1(b and c), occurred because the Al atoms diffused from the β-phase into the α-grains. It is seen in Figure 1(d) that after the annealing for 30 hr, the Al-rich regions of the specimen expanded, and a dispersed barrier formed around them. In a time shorter than 30 hr, the share of volume climbed to 42.1%. It was found that several α-grain boundaries did not contain any β-phase. The microstructural results manifested that the annealing treatment drastically decreases the quantity and distribution of β-phase, leading to highly saturated α-grains. Some particles from the second phase which were found using SEM under different processing settings are displayed in Figure 2.

XRD analysis

In the microstructure following the annealing at 300°C for 10, 20, and 30 hr, the volume and shape of the second phase after annealing can change significantly from the as-cast microstructure. Fine particles or strips of the coarse β-$Mg_{17}Al_{12}$ phase are dispersed along the grain boundaries and throughout the Mg matrix, drastically reducing the total amount of this phase. It is believed that a second phase is precipitated and then dissolved during the annealing process of Mg alloy designated as AZ91 [19]. During the subsequent process of cooling, the β-$Mg_{17}Al_{12}$ phase precipitates from the α-Mg supersaturated solution and disperses as minute particles throughout the α-Mg matrix. After being homogenized, the material underwent X-ray powder diffraction (XRD) pattern analysis, which elucidated that the $Mg_{17}Al_{12}$ phase diffraction peak was almost nonexistent in the substance (see Figure 3).

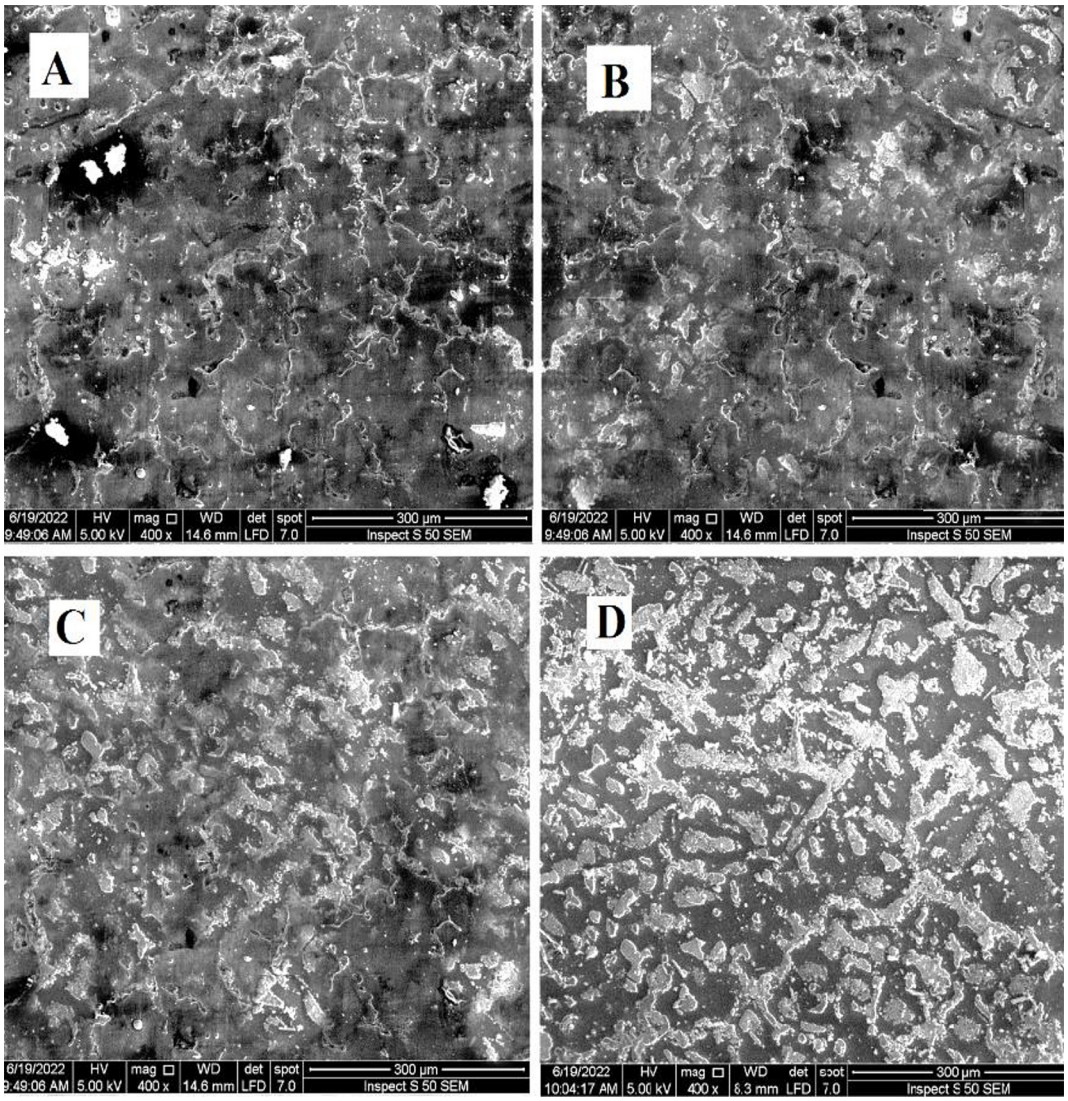

Figure 2. SEM analysis of the AZ91 alloy at: (a) at 0 hr; (b) 10 hr; (c) 20 hr; and (d) at 30 hr

Annealing the material could result in the formation of a single-phase, supersaturated solid solution, as the results of this study reveal.

Figure shows the XRD patterns of the samples annealed at 300°C with different time. The percentage of Mg–Zn intermetallic phases is minimal, making it difficult to identify prominent peaks. However, by comparing with the literature, the peaks with lesser intensities were detected [20]. Following the heat treatment at 300 °C, the corresponding intensities were observed to have dropped, which is indicative of the reduced $MgZn_2$ phase. In contrast, the Mg_7Zn_3 phase is indicated by peaks. Clearly, one could comprehend it shows, after prolonged exposure to temperatures above 300 °C, a new intermetallic phase (Mg_7Zn_3) forms in the alloy. Therefore, in the present study at the grain boundaries of specimens black patterns resembling networks emerged. After annealing at 300 °C and 30hr are believed to be made of Mg_7Zn_3 phase.

The XRD pattern of AZ91 alloy demonstrates the presence of usual direction peaks of the α-Mg phase (direction peaks at 2θ = 32.6, 34.9, 37.2, 48.5 and 58.0 JCPDS 35–0821). In addition, the β-$Mg_{17}Al_{12}$ phase (primary peak noticed at 2θ = 36.1. Observation minor peaks detected at 2θ = 40.1, 41.9 and 43.7, JCPDS 73–1148, which is a frequently seen intermetallic compound for the Mg-Al series alloys, is identified in the XRD pattern of AZ91 alloy. The XRD pattern of pretreated AZ91 specimens display characteristic direction peaks of the brucite phase $Mg(OH)_2$ (main peaks detected at 2θ = 38.0, 50.9 and 58.6, a minor peak at 2θ = 32.8, JCPDS 07–0239. It is indication that a bruited $Mg(OH)_2$ conversion surface layer is deposited on the Mg alloy after the annealing treatment. Heat treatment effects

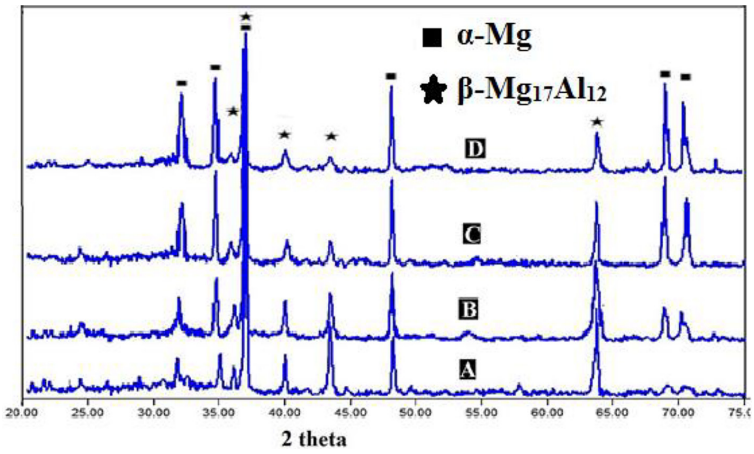

Figure 3. XRD patterns of the samples at: (A) 0 hr; (B) 10 hr; (C) 20 hr; and (D) 30 hr

on the crystal orientation of magnesium alloy by X-ray diffraction and suggested that the texture intensity of magnesium alloy before and after annealing changed slightly

Corrosion behavior

As cast, The Mg aluminum alloys that decompose have a characteristic microstructure consisting of three components: The eutectic structure, which consists of the alternating layers of phases; the α-Mg phase, and the β-$Mg_{17}Al_{12}$ phase. It has been determined that the β-$Mg_{17}Al_{12}$ phase is critical for managing the corrosion resistance of biodegradable Mg-Al alloys; hence, it is subjected to severe treatment. Micro galvanic corrosion cathodes can be revealed in the β-$Mg_{17}Al_{12}$ phase, which has a substantially higher Al concentration than the other phases. One of the most important aspects of the mechanism through which the corrosion occurs is the dispersion of the β-$Mg_{17}Al_{12}$ phase throughout the material. According to the research that has been conducted on corrosion resistance, the heat treatment has the potential to improve the corrosion resistance of the material by modifying the distribution, size, volume fraction, and configuration of amorphous $Mg_{17}Al_{12}$ precipitates. The corrosion-related behavior of Mg-Al alloys is greatly influenced by the fractional volume and the spatial distribution of these precipitates [21].

The corrosion behavior of the annealed samples surfaces exposed to heating for 10, 20, and 30 hr were carefully investigated by optical microscopy to acquire a deeper understanding of the impact by applying heat on the corrosion mechanism. Figures 4, 5, and 6 depict the micrographs captured using an optical microscope.

All the samples are plotted on a potentiodynamic polarization curve in Figure 7. and the electrochemical parameters of as-cast in comparison with heat-treated alloys in different solution shown in Table 2.

Figure 7(a) portrays the potentiodynamic polarization curves of each sample in a lactic acid solution. The corrosion rate was determined using the Tafel slope and electrochemical test conditions. The density of corrosion current (I_{corr}) decreased in all samples subjected to heat treatment. Both the corrosion potential (E_{corr}) and the corrosion current (I_{corr}) of the 30-hour heat-treated sample are greater than those of the untreated sample. Similarly, the samples taken at 0 hr exhibited larger values for (I_{corr}). Estimations of corrosion rates demonstrated that the longer annealing durations enhance the corrosion resistance of samples that have been heated.

The corrosion current density (I_{corr}) is illustrated to be reduced in the all heat-treated samples in Figure 7(b). The corrosion potential (E_{corr}) of the 30-hr heat-treated sample is superior to that of the 10-hr and 20-hr samples although the (I_{corr}) is greater. The 0-hr (I_{corr}) was also measured due to the higher corrosion current density it exhibited.

The effective dynamic polarization curves for all samples in the Ringer's solution are manifested in Figure 7(c). As measured along the Tafel Slope, the corrosion current density of all heat-treated samples was lower. This solution had the highest corrosive current density and corrosion potential after 20 hr of testing. After 0 hr, the current density was at its maximum, but it decreased for 10 hr and 30 hr of testing.

The galvanic corrosion occurring due to the iron impurity is clearly evident in the lactic solution.crevice corrosion associated with the

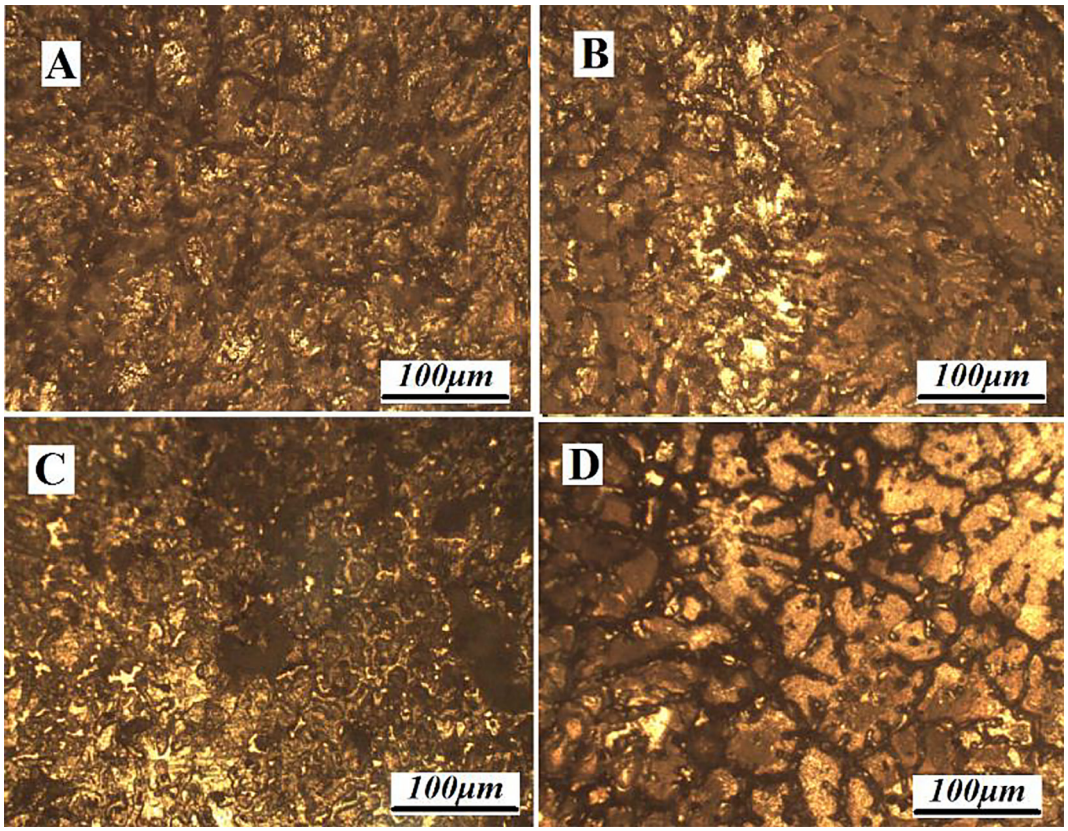

Figure 4. Optical microscopic micrographs showing the corroded morphologies of the samples of AZ91 in lactic solution: (a) 0 hr, (b) 10 hr, (c) 20 hr, and (d) 30 hr

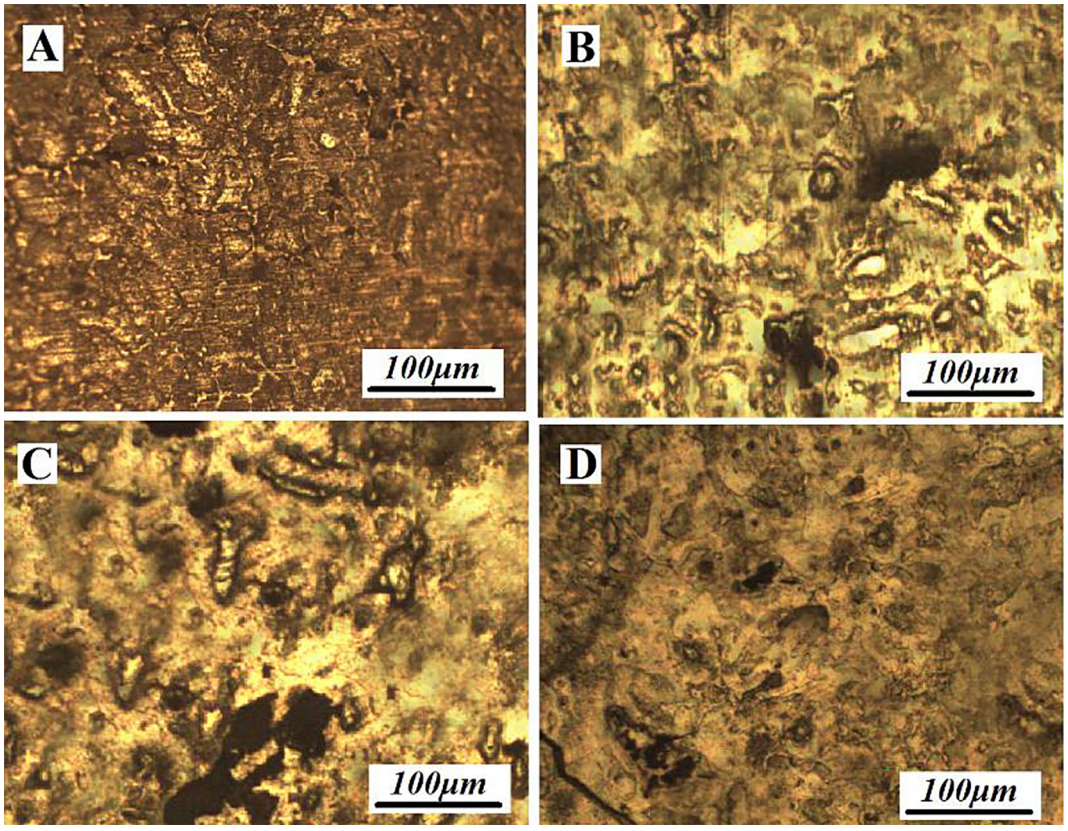

Figure 5. Optical microscopic micrographs showing the corroded morphologies of the samples AZ91 in SPF: (a) 0 hr, (b) 10 hr, (c) 20 hr, and (d) 30 hr

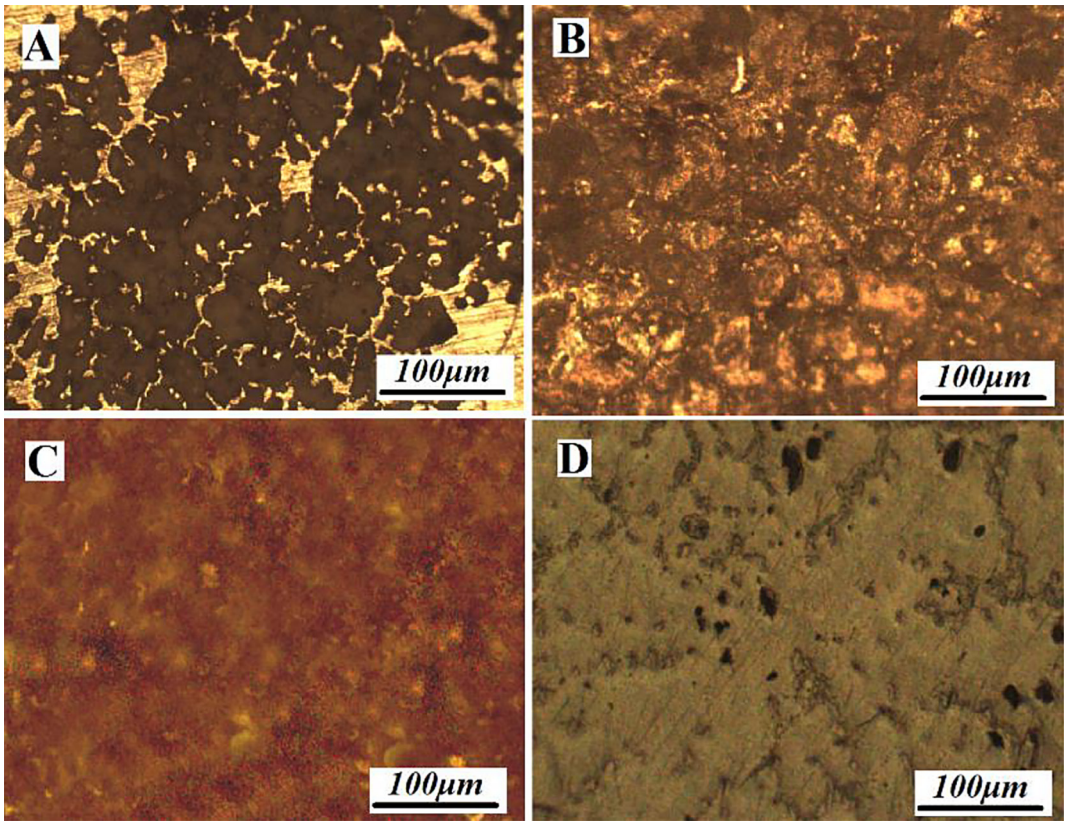

Figure 6. Optical microscopic micrographs showing the corroded morphologies of the samples AZ91 in a Ringer solution: (a) 0 hr, (b) 10 hr, (c) 20 hr, and (d) 30 hr

impurity in the magnesium matrix is displayed in the SBF solution it is develops in to pitting. General corrosion appears in the Ringer solution and develops in to pit corrosion as shown in (Figure 4, 5, and 6) formation of spherical corrosion morphology. The spherical corrosion morphology suggests formation of a hydrogen gas bubble at the corrosion site, as hydrogen evolution is usually associated with dissolution of magnesium ions. The hydrogen gas bubble separates the neighboring alloy surface from the corrosion site, with the impurity. Hence, the alloy surface inside the bubble is inhibited from corrosion. The preferential dissolution of the α-Mg matrix is facilitated due to the pH gradient formed at the interface of the hydrogen gas bubble and the alloy surface, thereby developing a spherical corrosion morphology, with the corrosion product deposited on the interface [22].

Microhardness results

Figure 8 elucidates the outcomes of microhardness tests conducted on all specimens subjected to a variety of heat treatments. The microhardness measurements from a (0 hr) sample (untreated) exhibit a wide distribution of variation. As a result of the existence of three completely separate regions (α, β, and α+β zones), this is the case. At 0 hr, the sample was measured to have a hardness of 73 HV0.5. After 10 hr of heat treatment decrease to 66 HV0.5, it was found that the

Table 2. Electrochemical parameters obtained from the polarization curves

Parameter	Ringer solution		SBF solution		lactic solution	
	Current [mA]	Potential [mV]	Current [mA]	Potential [mV]	Current [mA]	Potential [mV]
As cast AZ91	2.52823	-1034.48	0.135031	-1334.27	0.939026	-1304.5
AZ91–10hr	0.002545	-1068.02	0.020837	-1199.96	0.025694	-1264.7
AZ91–20hr	0.002122	-898.896	0.017635	-1358.36	0.013356	-1205.18
AZ91–30hr	0.273287	-929.895	0.019492	-882.704	0.012701	-1122.96

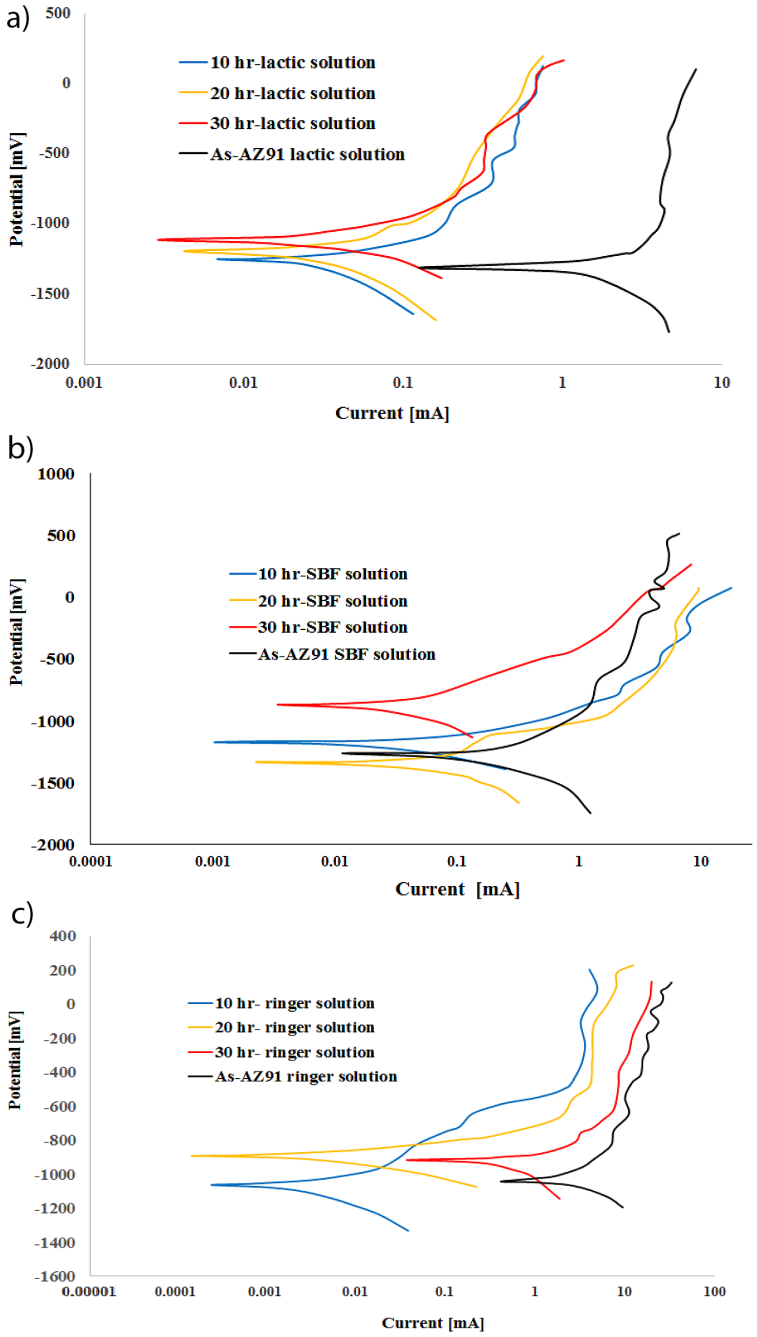

Figure 7. Potentiodynamic polarization curves of the specimens immersed by: (a) lactic, (b) SBF, and (c) Ringer's solution.

variation present within the heat-treated samples significantly decreased. In addition, after 20 hr was reached to 65 HV0.5 and after 30 hr of heat treatment hardness decrease slightly reduced to 64.5 HV0.5. One of the best ways to acquire a sound understanding of this topic is to investigate the microstructure of samples. The heat treatment of the samples resulted in an overall reduction in hardness, which was caused by a decrease in the hard and brittle phases ($Mg_{17}Al_{12}$) as well as the eutectic areas. This was a substantial contributor to the overall decrease in hardness, since the Mg AZ91 alloy exhibits both hard and soft phases in various regions. The hardness of the β-phase was greater than that of the other phases, according to measurements [23]. It was found that the hardness decreased when approaching the eutectic area or α-phase. Consequently, the untreated AZ91 showed larger hardness variations. This research indicates that by applying the heat, the β-phase and eutectic zones may be reduced, and the α-grains can become supersaturated. Thus,

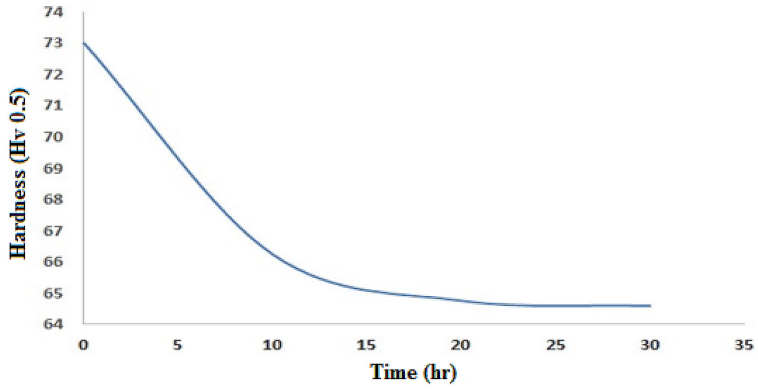

Figure 8. Effect of annealing time on hardness values for AZ91 Mg alloys

it can be seen from Figure 8 that the differences were found to be reduced following the heat treatment. In addition to the extent to which a second phase is present, the creation of supersaturated grains and the alteration of the average grain size are also key factors in determining the final hardness of material following the heat treatment. The formation of supersaturated grains increases the hardness, whereas the decrease in the secondary phase and the grain development reduces it. Due to the interaction of these three factors, the hardness of a material that was heated slightly dropped. This research shows that the supersaturated grains formation contributes less to the secondary phase and the grain expansion, hence reducing the hardness.

Figure 1(A) depicts that the microstructures of the as-cast Mg alloy are characterized by the uneven network structures with the serious segregations, and the eutectics are distributed mainly along crystal boundary. After the annealing treatment for 10 hr Figure 1(B), the structure of the as-cast Mg alloy is uniform, and the segregation is eliminated. Also, after the annealing treatment for 20 hr Figure 1(C), the majority of eutectics are dissolved during the annealing. In Figure 1(D), a portion of the quadratic phase is precipitated into irregular-petal distribution along the crystal boundary, which is accompanied by the formation of twins. And, for a long time (30 hr), the quadratic-phase precipitation increases, the twins become big, and the structure turns into a network distribution (Figure 1(D)). In the Mg AZ91 alloy during the casting process, the β-$Mg_{17}Al_{12}$ phase precipitates from supersaturated α-Mg, and a number of α phases discontinuously precipitated along the crystal-grain boundary as well as continuously precipitated inside the crystal grain. In addition, the precipitated α phase is apparently smaller than that of the as-cast alloy and its morphological structure changes greatly. As the annealing process continues, the alloy hardness indicator declines significantly; under the annealing condition of 20–30 hr, the alloy hardness is even

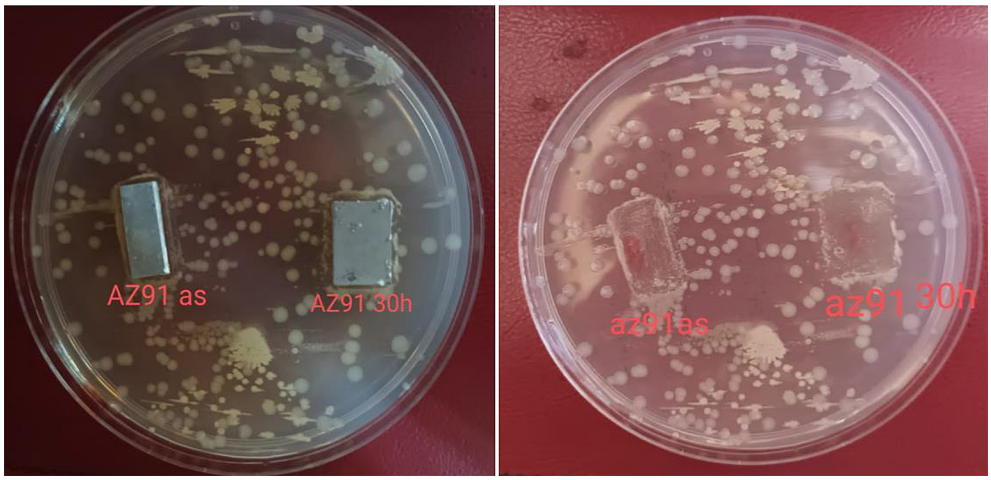

Figure 9. Images for *E. coli* bacteria

Table 3. Percentage of killing bacteria *E. coli*

Sample	Bacterial rate % of AZ91
As received	1
After annealing (30 h)	2

lower than that of the alloy in its as-cast state. This is because, as the annealing process continues, the β-$Mg_{17}Al_{12}$ is soft at 20–30°C, and it has no pinning effect on the crystal-grain boundary, making the alloy possess a comparatively higher toughness and lower hardness.

Antibacterial assessment

The initiation of microbial colonization, persistence, and concurrent infection are all the risks associated with the biomaterial surfaces. Due to the potential importance of this research in the medical field, an assessment of the antibacterial properties of composite materials was required. An antimicrobial agent's mode of action for killing the bacteria can vary with the type of bacteria that are targeting. Using the inhibition zone strategy, more about the antibacterial inhibition zone (N. agar method) was learned, as evinced in Figure 9. According to the results, the samples significantly inhibited the growth of E. coli. The test specimens are divided into two halves: The as-received Mg alloy AZ91 alloy and the Mg alloy AZ91 annealed at 300 °C for 10, 20 and 30 h [24].

The fact that the AZ91 in heat treatment inhibits the microorganisms better than the as-received AZ91, and this is likely attributable to the chemical composition of alloy, as the high Al percentage (8.97) in the alloy, the absence of antibacterial activity in Al, and the ease with which the microorganisms can proliferate on the Al surfaces. The amount of zinc in the alloy is 0.58%, whereas the amount of magnesium is 90.103%. Table 3 lists the results for this strategy as a percentage of fatalities.

Activity against bacteria exhibited by certain substances that release metal ions (Cu^{2+}, Zn^{2+}, Al^{+} … etc.) involves main unique elements, as following: In the first place, metal ions on the surface establish strong interactions with amino and carboxyl groups of the bacterial membrane and proteins, which disables them and leads to structural alterations. Second, a bacterial membrane that has undergone structural changes shows a significant increase in permeability, preventing the bacteria from performing accurate monitoring of the transport occurring across the plasma membrane. In the final stage, metal ions interact with the nucleic acids of bacteria, which ultimately results in the death of the cells by blocking replication [25].

CONCLUSIONS

To determine how the microstructure change of Mg AZ91 alloy impacts its corrosion resistance, the material was heat treated at 300 °C for 10, 20, and 30 h. The following conclusions can be drawn from the data. The volume and distribution of the secondary phase ($Mg_{17}Al_{12}$) at the grain boundaries of Mg AZ91 alloy were drastically altered by heat annealing. As the annealing hours increase, the $Mg_{17}Al_{12}$ phase gradually decreases. When the homogenized Mg AZ91 alloy was annealed at 300°C for 10, 20, and 30 hr, the β-$Mg_{17}Al_{12}$ phase was greatly reduced by being dispersed in a line along the grain borders and in the α-Mg matrix as minute strips or particles. The Mg AZ91 alloy was homogenized during the annealing, and its corrosion resistance much improved. The average hardness of the material after heat treatment was comparable to that of untreated Mg AZ91 alloy, however, the range of hardness values greatly reduced.

After the heat treatment, the supersaturated grains, which promoted a greater rate of corrosion, substantially decreased the corrosion resistance. According to the findings of this study, the corrosion resistance of Mg AZ91 alloy can be improved with adequate heat treatment; nevertheless, if the structure is to function in a corrosive environment, the heat treatment must be performed with a great care.

All samples heat treated by annealing showed the best corrosion resistance in all solutions compared to the untreated samples. The best annealing temperature in terms of corrosion resistance was obtained for heat-treated samples for 30 hours in lactic solution, 10 hours in SBF solution, and 20 hours in Ringer solution. The heat treatment and the composite demonstrated only a poor antibacterial action against the gram-negative E. coli, with a correspondingly limited zone of bacterial suppression in the 30-hr sample (2 mm).

REFERENCES

1. Fiorentini D., Cappadone C., Farruggia G., Prata C. Magnesium: Biochemistry, Nutrition, Detection, and Social Impact of Diseases Linked to Its Deficiency. Nutrients. 2021; 13(4): 1136.
2. Xu L., Liu X., Sun K., Fu R., Wang G. Corrosion Behavior in Magnesium-Based Alloys for Biomedical Applications. Materials. 2022; 15(7): 2613.
3. Zhang Y., Zimmermann T., Mueller W.-D., Witte F., Beuer F., Schwitalla A. Exploring the degradation behavior of MgXAg alloys by in vitro electrochemical methods. Bioactive Materials. 2021; 7.
4. Ślęzak M., Bobrowski P., Rogal L. Microstructure Analysis and Rheological Behavior of Magnesium Alloys at Semi-solid Temperature Range. Journal of Materials Engineering and Performance. 2018; 27.
5. Szklarz Z., Rogal Ł. Influence of heat treatment on the microstructure and corrosion behavior of Thixocast Mg-Y-Nd-Zr. Journal of Materials Engineering and Performance. 2020; 29(9): 6181–6195.
6. Baslayici S., Bugdayci M., Benzesik K., Yucel O., Acma M.E. Corrosion behavior of hydroxyapatite coated AZ31 and AZ91 Mg alloys by electrostatic spray coating. International Journal of Materials Research. 2022; 113(2): 93–100.
7. Jana A., Das M., Balla V.K. Effect of heat treatment on microstructure, mechanical, corrosion and biocompatibility of Mg-Zn-Zr-Gd-Nd alloy. Journal of Alloys and Compounds. 2020; 821: 153462.
8. Fujisawa S., Yonezu A., editors. Mechanical property of microstructure in die-cast magnesium alloy evaluated by indentation testing at elevated temperature. Recent Advances in Structural Integrity Analysis–Proceedings of the International Congress (Apcf/Sif-2014); 2014.
9. Iwaszko J., Strzelecka M. Microstructure and Corrosion Resistance of AZ91 Magnesium Alloy after Surface Remelting Treatment. Materials (Basel, Switzerland). 2022; 15(24).
10. Zhang Y., Liu W., Liu Y., Zhang M., Tian Y., Chen L. Research Progress on Corrosion Behaviors and Improvement Methods of Medical Degradable Mg− Based Alloys. Metals. 2022; 13(1): 71.
11. Mena-Morcillo E., Veleva L. Degradation of AZ31 and AZ91 magnesium alloys in different physiological media: Effect of surface layer stability on electrochemical behaviour. Journal of Magnesium and Alloys. 2020; 8(3): 667–75.
12. Pogorielov M., Husak E., Solodivnik A., Zhdanov S. Magnesium-based biodegradable alloys: Degradation, application, and alloying elements. Interventional Medicine & Applied Science. 2017; 9(1): 27–38.
13. Li T., Sun F., Zhao Y., Chen M. The corrosion resistance of SiO2-hexadecyltrimethoxysilane hydrophobic coating on AZ91 alloy pretreated by plasma electrolytic oxidation. Progress in Organic Coatings. 2023; 174: 107232.
14. Panahi Z., Tamjid E., Rezaei M. Surface modification of biodegradable AZ91 magnesium alloy by electrospun polymer nanocomposite: Evaluation of in vitro degradation and cytocompatibility. Surface and Coatings Technology. 2020; 386: 125461.
15. Iranshahi F., Nasiri M.B., Warchomicka F.G., Sommitsch C. Corrosion behavior of electron beam processed AZ91 magnesium alloy. Journal of Magnesium and Alloys. 2020; 8(4): 1314–27.
16. Thakur A., Gharde S., Kandasubramanian B. Electroless nickel fabrication on surface modified magnesium substrates. Defence Technology. 2019; 15(4): 636–44.
17. Amukarimi S., Mozafari M. Biodegradable Magnesium Biomaterials–Road to the Clinic. Bioengineering. 2022; 9(3): 107.
18. V S.C., Dumpala R., S A.K., Vv K., B R.S. Influence of heat treatment on the machinability and corrosion behavior of AZ91 Mg alloy. Journal of Magnesium and Alloys. 2018; 6(1): 52–8.
19. Robson J.D., Stanford N., Barnett M.R. Effect of precipitate shape on slip and twinning in magnesium alloys. Acta Materialia. 2011; 59(5): 1945–56.
20. Li L., Jiang W., Guo P.-T., Yu W.-B., Wang F., Pan Z.-Y. Microstructure evolution of the Mg-5.8 Zn-0.5 Zr-1.0 Yb alloy during homogenization. Materials Research. 2017; 20: 1063–71.
21. Mohammadi Zerankeshi M., Alizadeh R., Gerashi E., Asadollahi M., Langdon T.G. Effects of heat treatment on the corrosion behavior and mechanical properties of biodegradable Mg alloys. Journal of Magnesium and Alloys. 2022.
22. Abdalla M., Joplin A., Elahinia M., Ibrahim H. Corrosion modeling of magnesium and its alloys for biomedical applications. Corrosion and Materials Degradation. 2020; 1(2): 11.
23. Sunil B.R., Ganesh K., Pavan P., Vadapalli G., Swarnalatha C., Swapna P., et al. Effect of aluminum content on machining characteristics of AZ31 and AZ91 magnesium alloys during drilling. Journal of Magnesium and Alloys. 2016; 4(1): 15–21.
24. Brooks E.K., Ahn R., Tobias M.E., Hansen L.A., Luke-Marshall N.R., Wild L., et al. Magnesium alloy AZ91 exhibits antimicrobial properties in vitro but not in vivo. Journal of biomedical materials research Part B, Applied Biomaterials. 2018; 106(1): 221–7.
25. Lin Z., Sun X., Yang H. The Role of Antibacterial Metallic Elements in Simultaneously Improving the Corrosion Resistance and Antibacterial Activity of Magnesium Alloys. Materials & Design. 2021; 198: 109350.